Sensors and Actuators B 266 (2018) 213–220

Contents lists available at ScienceDirect

Sensors and Actuators B: Chemical

journal homepage: www.elsevier.com/locate/snb

Highly sensitive and selective triethylamine gas sensor based on porous SnO_2/Zn_2SnO_4 composites

Xueli Yang [a], Qi Yu [a], Sufang Zhang [a], Peng Sun [a,*], Huiying Lu [a], Xu Yan [a], Fangmeng Liu [a], Xin Zhou [b,c], Xishuang Liang [a], Yuan Gao [a], Geyu Lu [a,*]

[a] State Key Laboratory on Integrated Optoelectronics, College of Electronic Science and Engineering, Jilin University, 2699 Qianjin Street, Changchun 130012, China
[b] International Center for Materials Nanoarchitectonics (WPI-MANA), National Institute for Materials Science(NIMS), 1-1 Namiki, Tsukuba, Ibaraki 305-0044, Japan
[c] Graduate School of Pure and Applied Sciences, University of Tsukuba, 1-1-1 Tennodai, Tsukuba, Ibaraki 305-8577, Japan

ARTICLE INFO

Article history:
Received 11 January 2018
Received in revised form 7 March 2018
Accepted 11 March 2018
Available online 12 March 2018

Keywords:
SnO_2/Zn_2SnO_4
Triethylamine
Hydrothermal method
Gas sensor

ABSTRACT

In this work, hierarchical porous SnO_2/Zn_2SnO_4 composites were synthesized via a facile one-step hydrothermal method with subsequent heat treatment. Many methods were performed to investigate the crystalline and morphological characterization of the as-prepared composite. The gas sensors based on the porous SnO_2/Zn_2SnO_4 composite were fabricated and their gas sensing performance was systematically investigated. Significantly, compared with the pure SnO_2 and Zn_2SnO_4 solid particles, the hierarchical SnO_2/Zn_2SnO_4 porous spheres exhibited excellent gas sensing properties toward triethylamine (TEA). The response value was 48 toward 100 ppm TEA, and the detection limit could be down to 500 ppb with a response value of 1.4. The excellent gas sensing properties are contributed to the porous nanostructure and the heterojunction between SnO_2 and Zn_2SnO_4 composite.

1. Introduction

Triethylamine (TEA), as an explosive and inflammable gas, can cause great damage on human health and environment, such as eye and skin burns, headaches and especially respiratory difficulty [1–4]. Therefore, it is necessary to detect and monitor the concentration of TEA in the air. Up to now, many methods have been explored to achieve the detection and monitoring TEA, including gel chromatography techniques, electro-chemistry analysis, and colorimetric method [5–7]. Though these methods have high precision and good stability, however, they also have complicated detection process, long detection period and expensive equipment, which have limited them into practical application. Therefore, it is significant to develop an accurate and fast detection method for TEA with high sensitivity, good selectivity and low detection limit.

Metal oxide semiconductor gas sensors have been demonstrated as a kind of sensor with advantages of high sensitivity, low cost, low power consumption and real-time operation [8–11]. Previous researches revealed that the gas sensing properties of oxide semiconductors were closely related with their compositions, crystalline sizes, and surface morphologies [12–15]. Zn_2SnO_4 as an *n*-type semiconductor oxide with a wide band gap of 3.6 eV at room temperature is a transparent conducting oxide with high electron mobility, low visible adsorption, and high electrical conductivity. Therefore, it has been widely used in the areas of solar cells [16–18], photocatalysts [19–21], lithium ion batteries [22–24] and gas sensors [25–28]. As known, the gas sensors based on the Zn_2SnO_4 composite exhibit good sensing properties to many volatile organic chemicals (VOCs), such as ethanol, acetone, formaldehyde and toluene [29–33], however, as far as we know the research on Zn_2SnO_4 material for the detection of TEA has been rarely reported [34].

Herein, porous SnO_2/Zn_2SnO_4 composites were prepared through a facile hydrothermal method with subsequent calcination processes. Gas sensing performances of sensors based on the as-prepared products were evaluated and systematically investigated. Compared with pure SnO_2 and Zn_2SnO_4 solid particles, the porous SnO_2/Zn_2SnO_4 composites exhibited excellent gas sensing properties toward TEA at the optimum temperature of 250 °C, giving a response of 48–100 ppm TEA. Moreover, the sensor also showed fast response, super selectivity and a low detection limit (500 ppb).

* Corresponding authors.
E-mail addresses: pengsun@jlu.edu.cn (P. Sun), lugy@jlu.edu.cn (G. Lu).

https://doi.org/10.1016/j.snb.2018.03.044
0925-4005/

2. Experimental section

2.1. Synthesis process

All reagents used in this experiment were of analytical grade and directly used without any further purification.

The porous SnO_2/Zn_2SnO_4 composite was synthesized through a hydrothermal method. In a typical process, 1 mmol of $Na_2SnO_3{\cdot}4H_2O$ and 0.06 g of sodium alginate were dissolved in 10 mL of deionized water (named as solution A). 2 mmol of Zn $(CHCOO)_2{\cdot}2H_2O$ was dissolved in 2 mL of deionized water, and then added with 5 mL of ammonia hydroxide (named as solution B). After about 15 min, solution B was mixed with solution A with stirring for another 30 min at room temperature. Then the mixed solution was transferred into a 50 mL of Teflon-lined autoclave and heated at 160 °C for 6 h. After the autoclave cooled down to room temperature, the product was collected by centrifugation, washed with deionized water and ethanol for several times, respectively, and dried in air at 80 °C for 12 h. The product was then annealed at 800 °C for 30 min in air with a heating rate of 5 °C/min to obtain SnO_2/Zn_2SnO_4 composites. The SnO_2 solid particles used in this work were of analytical grade commercial SnO_2 particles, and the Zn_2SnO_4 particles used in this work were synthesized through a hydrothermal method, the synthetic process of Zn_2SnO_4 solid particles was described in supporting information.

2.2. Characterization

The phase characterization of SnO_2/Zn_2SnO_4 composite was characterized by X-ray powder diffraction (XRD) on a Rigaku D/Max–2550 V diffractometer using Cu-Kα radiation (λ = 1.54178 Å). The morphology and composition of the product were investigated by field emission scanning electron microscopy (FESEM) on a JSM-7500F (JEOL) microscope operating at an accelerating voltage of 15 kV, Transmission electron microscopy (TEM) and high-resolution transmission electron microscopy (HRTEM) observations were carried out on a JEM-2200FS apparatus (JEOL) operating at 200 kV. Elemental mapping analysis was performed by the energy dispersive X-ray spectrometry (EDS) by the TEM attachment.

2.3. Fabrication and measurement of gas sensor

The sensor fabrication and the measurement system are referred to the literature process [9]. An alumina ceramic tube was selected with the length, external diameter and internal diameter of 4, 1.2, and 0.8 mm, respectively, and a pair of gold electrodes was attached on the end of the tube. The as-synthesized SnO_2/Zn_2SnO_4 composite was mixed with deionized water to form a paste, and then coated onto the ceramic tube with a small brush to form a thick film. The device was dried at room temperature and calcined at 400 °C for 2 h. A Ni-Cr alloy coil heater was inserted into the alumina ceramic tube. The operating temperature was controlled by adjusting the heating current. The schematic diagram of the sensor device is illustrated in Fig. 1.The gas sensing properties were measured by using a RG-2 gas sensing characterization system under laboratory condition (30 RH%, 23 °C). The measurement was conducted by a static process. A given amount of the tested gas was injected into a closed glass chamber, and the sensor device was put into the chamber for the measurement of the sensing performance. The sensor response is defined as $S = R_a/R_g$, where R_a is the sensor resistance in the air, and R_g is the sensor resistance in the tested gas. The response time (τ_{res}) and recovery time (τ_{recov}) were defined as the time taken by the sensor to achieve 90% of the total resistance change in the case of adsorption and desorption, respectively. The operating temperature was varied between 200 and 350 °C.

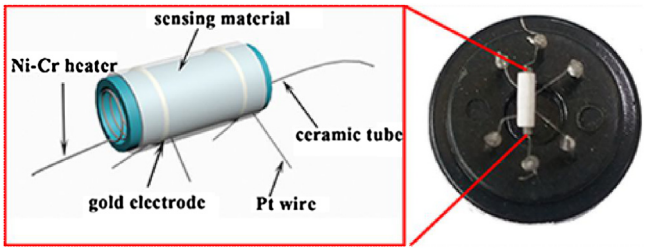

Fig. 1. Schematic diagram of the sensor device.

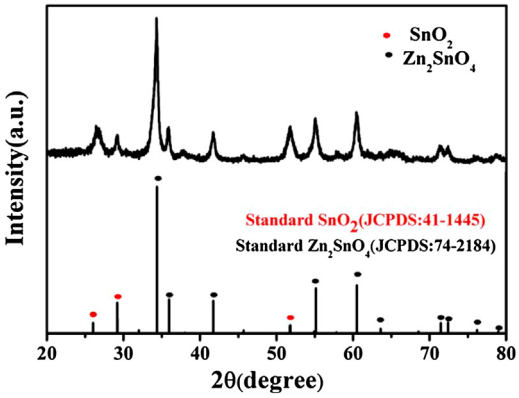

Fig. 2. XRD patterns of the as-prepared SnO_2/Zn_2SnO_4 composite.

3. Results and discussion

3.1. Structural and morphological characteristics

The phase and crystal structure of the SnO_2/Zn_2SnO_4 product were investigated by XRD. Fig. 2 is the representative XRD pattern obtained after annealing the precursor at 800 °C. From the XRD patterns, it can be clearly seen that most of the XRD peaks could be indexed to Zn_2SnO_4 and the rest peaks to SnO_2, which indicates that the product was a composite of Zn_2SnO_4 and SnO_2. Compared with the standard JCPDS cards, Zn_2SnO_4 and SnO_2 in the composite were in good agreement with the inverse spinel Zn_2SnO_4 (JCPDS: 74-2184) and tetragonal SnO_2 (JCPDS: 41-1445). Additionally, no other peaks could be found in the XRD patterns of SnO_2/Zn_2SnO_4 composite, indicating the high purity of the crystalline composite.

The morphology and surface structure of the sample were observed by FESEM and TEM. It can be seen in Fig. 3a that the as-prepared SnO_2/Zn_2SnO_4 composite had a sphere-like morphology and were uniformly dispersed with a rough surface. Fig. 3b is the SEM image of a single SnO_2/Zn_2SnO_4 sphere, it could be seen that the sphere with the diameter of about 200 nm was composed of many nanoparticles. The TEM images of Fig. 3c and d show more micro-structural details of the composite. It is clearly that the as-synthesized spheres had a porous microstructure which agreed well with the SEM observations. This porous structure may increase the specific surface area, and provide more surface active sites which will contribute to the improved sensing property. The SEM images of the pure SnO_2 and Zn_2SnO_4 solid particles were displayed in Fig. S1.

The HRTEM analysis of SnO_2/Zn_2SnO_4 composites is depicted in Fig. 4a–c. The HRTEM images of the selected area marked with white rectangles in Fig. 4a indicated the lattice fringe spacing of 0.261 nm corresponding to the spacing of the (311) lattice plane of inverse spinel Zn_2SnO_4 (Fig. 4b), and 0.334 nm correspond-

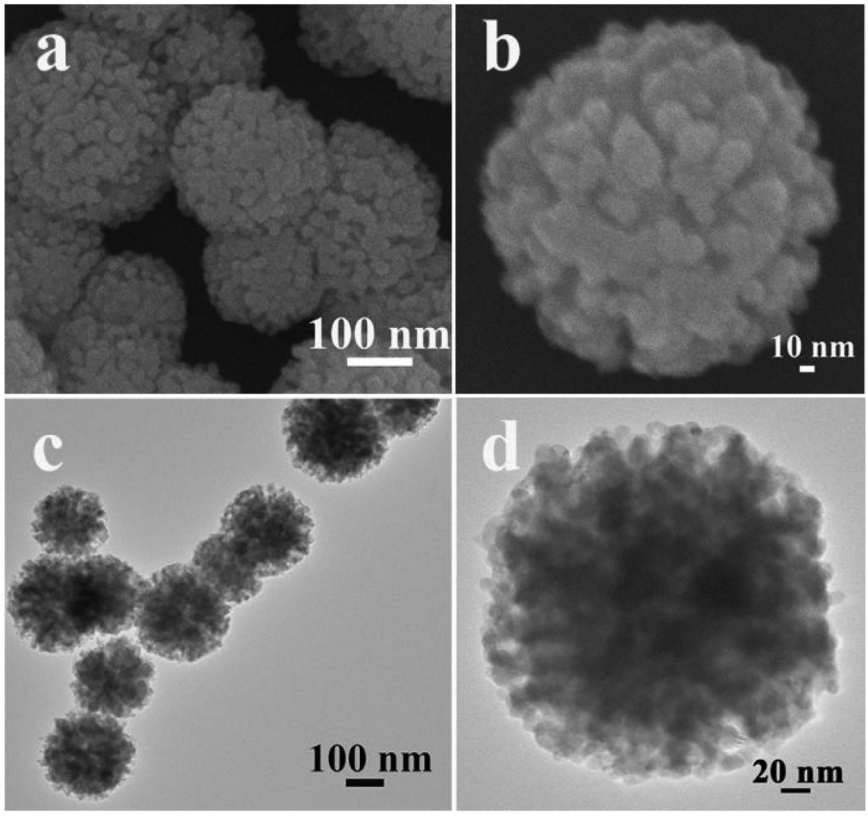

Fig. 3. (a and b) FESEM and (c and d) TEM images of the SnO_2/Zn_2SnO_4 spheres.

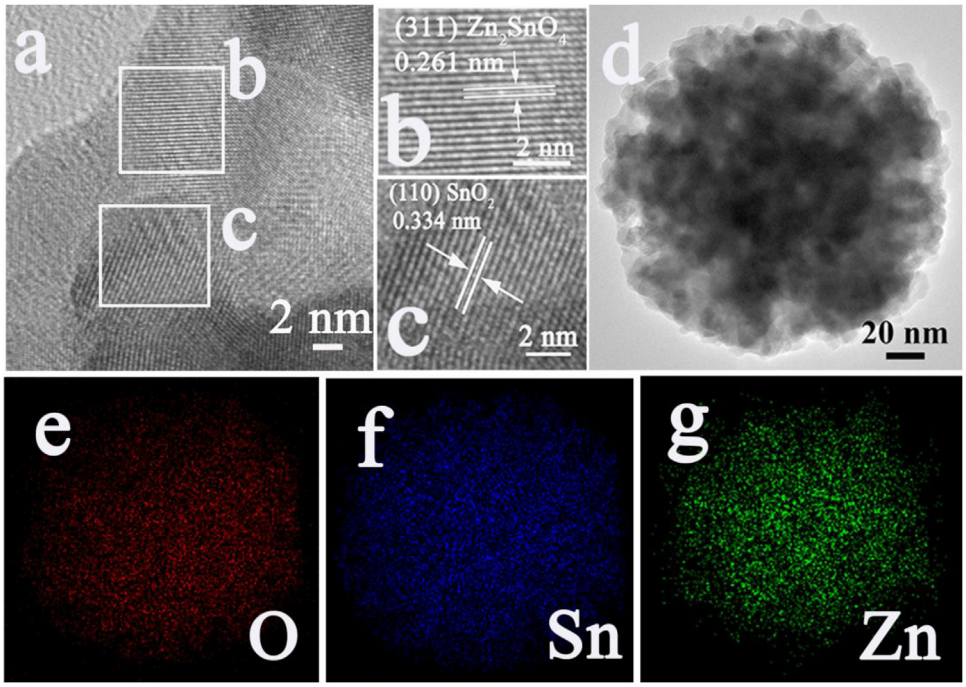

Fig. 4. (a–c) HRTEM, (d) TEM, and (e–g) Elemental mapping images of the composite.

ing to the spacing of the (110) lattice plane of tetragonal SnO_2 (Fig. 4c). TEM elemental mapping images corresponding to a single SnO_2/Zn_2SnO_4 sphere (Fig. 4d) was applied to illustrate the spatial distributions of Zn, Sn and O elements in the sample of the SnO_2/Zn_2SnO_4 composite. It can be clearly seen that O, Sn and Zn were homogeneously distributed in SnO_2/Zn_2SnO_4 composite, as shown in Fig. 4e–g.

3.2. Gas sensing characteristics

The gas sensors based on the pure SnO_2, Zn_2SnO_4 solid particles and porous SnO_2/Zn_2SnO_4 spheres were fabricated and the responses of the gas sensors to TEA were measured as a function of operating temperature. The corresponding bar graph is shown in Fig. 5a, all of the three sensors showed an “increase-maximum-

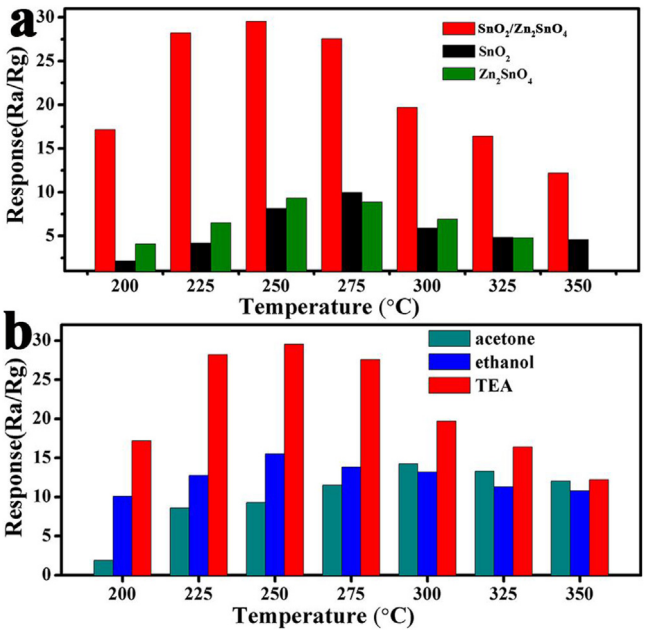

Fig. 5. (a) Responses of the gas sensors based on SnO_2 and Zn_2SnO_4 solid particles to 100 ppm TEA and the porous SnO_2/Zn_2SnO_4 spheres to 50 ppm TEA. (b) Response of the gas sensor based on porous SnO_2/Zn_2SnO_4 spheres to acetone and ethanol of 100 ppm, and TEA of 50 ppm.

decrease" tendency. The highest response value toward TEA could be observed of the sensor based on the porous SnO_2/Zn_2SnO_4 spheres, and the maximum response was 29.5 toward 50 ppm TEA at the operating temperature of 250 °C. For the sensors based on SnO_2 and Zn_2SnO_4 solid particles the maximum response toward 100 ppm TEA was reached at 9.9 and 9.3, respectively. Obviously, the sensor based on the porous SnO_2/Zn_2SnO_4 spheres exhibited better response toward TEA. Then, the gas sensing response of the sensor based on the porous SnO_2/Zn_2SnO_4 spheres toward TEA, ethanol and acetone was investigated as a function of operating temperature, as depicted in Fig. 5b. It can be observed that the response of the sensor varied with operating temperature and exhibited a temperature-dependent feature. As can be seen in Fig. 5b that the sensor showed the highest response to 50 ppm TEA with the temperature ranged from 200 °C to 350 °C. However, the maximum response value of the sensor toward TEA of 50 ppm was 29.5 at 250 °C, while the response value to ethanol and acetone with a concentration of 100 ppm was only 15.5 and 14.2, respectively, which was only half of the response value to TEA, and 250 °C was chosen as the optimum operating temperature to further evaluate the sensing performance of the sensor toward TEA.

The dynamic responses of the gas sensors were explored when orderly exposed to different concentrations of TEA at 250 °C, (Fig. 6). It can be seen in Fig. 6b that the response increased with the TEA concentration ranging from 500 ppb to 5 ppm, the responses were 1.4, 1.6, 2.2, 3.2, 3.7 and 4.3, respectively. And then with the TEA concentration changed from 10 to 50 ppm, the corresponding responses were 13.1, 19.6, 22.0, 24.3, and 29.5, respectively (Fig. 6c). Fig. 6a and the inset is the corresponding linearity curve of the gas sensing responses toward TEA with different concentration. Clearly, the sensor displayed an approximately linear increase with the concentration of TEA increased from 500 ppb to 5 ppm, and 10 ppm to 50 ppm. The sensing performances comparison between the as-prepared SnO_2/Zn_2SnO_4 spheres and literature results is summarized in Table 1 [34–39]. It is worth noting that the sensor based on SnO_2/Zn_2SnO_4 spheres has relatively better gas sensing performance toward TEA than that of the reported sensors, including lower detection limit, lower operating temperature, and higher sensing response.

Selectivity is a vital parameter of gas sensors for their practical application. The selectivity of the sensor based on pure SnO_2, Zn_2SnO_4 solid particles and porous SnO_2/Zn_2SnO_4 spheres were investigated as shown in Fig. 7. The bar graph of the responses of the sensors toward various kinds of volatile organic gases, including TEA, ethanol, acetone, methanol, formaldehyde, and toluene with a concentration of 100 ppm at their optimum operating temperature was listed. All of the three sensors showed the highest response to TEA, and a relatively lower response to other tested gases. For the sensors based on pure SnO_2, Zn_2SnO_4 solid particles the gas sensing response toward TEA, ethanol and acetone had no significant difference, while the sensor based on the porous SnO_2/Zn_2SnO_4 spheres, the gas sensing response toward TEA was much higher than to the other tested gases. The responses to TEA, ethanol, acetone, methanol, formaldehyde and toluene were 48.2, 15.5, 9.7, 5.6 4.7 and 4.1. Obviously, the response value to TEA was 3–12 times higher than to the other tested gases, which indicated that the sen-

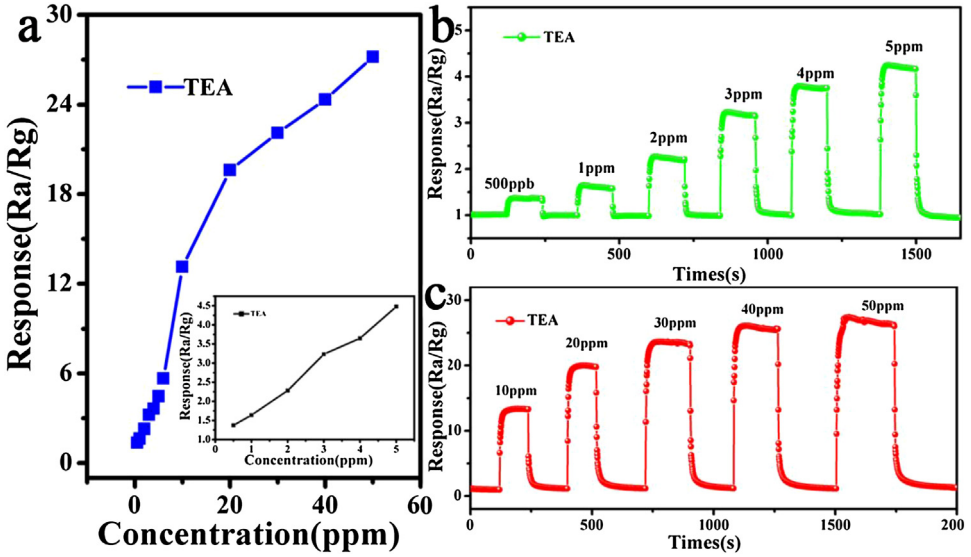

Fig. 6. (a) Response of the porous SnO_2/Zn_2SnO_4 spheres to different concentrations of TEA at 250 °C. (b and c) Response transients of porous SnO_2/Zn_2SnO_4 spheres to different concentrations of TEA at 250 °C.

Table 1
Comparison of TEA sensing performance of gas sensors based on other material in previous reports.

Sensing materials	Con. (ppm)	Tem. (°C)	Res. (R_a/R_g)	Det. Lim. (ppm)	Ref.
Polyhedral Zn_2SnO_4	100	200	37	5	[34]
ZnO nanorod	50	300	45	2	[35]
V_2O_5 hollow sphere	100	370	7.3	0.01	[36]
TiO_2 nanorod	50	290	9.5	0.1	[37]
SnO_2 microfibre	100	270	49.5	2	[38]
SnO_2 nanowire/ZnO nanorod	115	300	8.2	No	[39]
SnO2/Zn_2SnO_4 porous sphere	100	250	48	0.5	This work

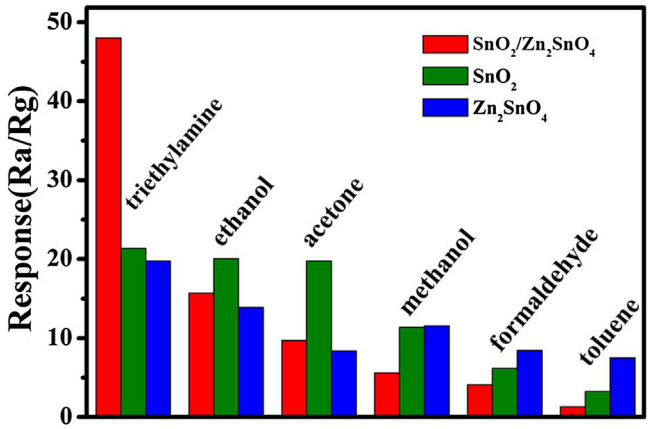

Fig. 7. Responses of the sensors to various test gases of 100 ppm at their optimum operating temperature.

sor based on porous SnO_2/Zn_2SnO_4 spheres had a high response and good selectivity to TEA.

Response and recovery characteristic is another important parameter of gas sensor. The response and recovery properties of the sensors to 20 ppm TEA were investigated, The response transients of the SnO_2/Zn_2SnO_4 sensor at 175 °C, 200 °C, 225 °C, 250 °C, 275 °C and 300 °C are displayed in Fig. 8(a–f). It can be seen that the resistance was significantly decreased with the increasing of operating temperature, moreover, the response and recovery time was also varied with different temperature. It could be also seen that the response and recovery time was reduced greatly with the increasing temperature, and at the optimal temperature of 250 °C, the response and recovery time was 2 s and 184 s, respectively. Fig. 8g displays the response and recovery time with the increase of temperature and also it can be observed that the response and recovery time was nearly linearly decreased with the operating temperature.

Since water vapor is an important interference factor to gas response, in order to evaluate the humidity effect, the TEA sensing tests were conducted under a RH of 20, 40, 60, 80 and 98%. Fig. 9a and b depicts the response transients of SnO_2/Zn_2SnO_4 under a RH of 20, 40, 60, 80 and 98%, respectively. Under all RH, the SnO_2/Zn_2SnO_4 sensor showed a relatively stable response to TEA. However, the response to TEA decreased with the increasing RH, and the resistance of the sensor also reduced with the RH change from 20 to 98%. As shown in Fig. 9c, the ratio of the gas response at 98% and 40% RH ($R_{gas,98\%RH}/R_{gas,40\%RH}$) was 0.91, which indicating that the RH did not much affect the sensing response to TEA. Studies have shown that under humid conditions, there is an interaction between water vapor and adsorbed oxygen ions, which results in the formation of terminal hydroxyl groups on the sensing material,

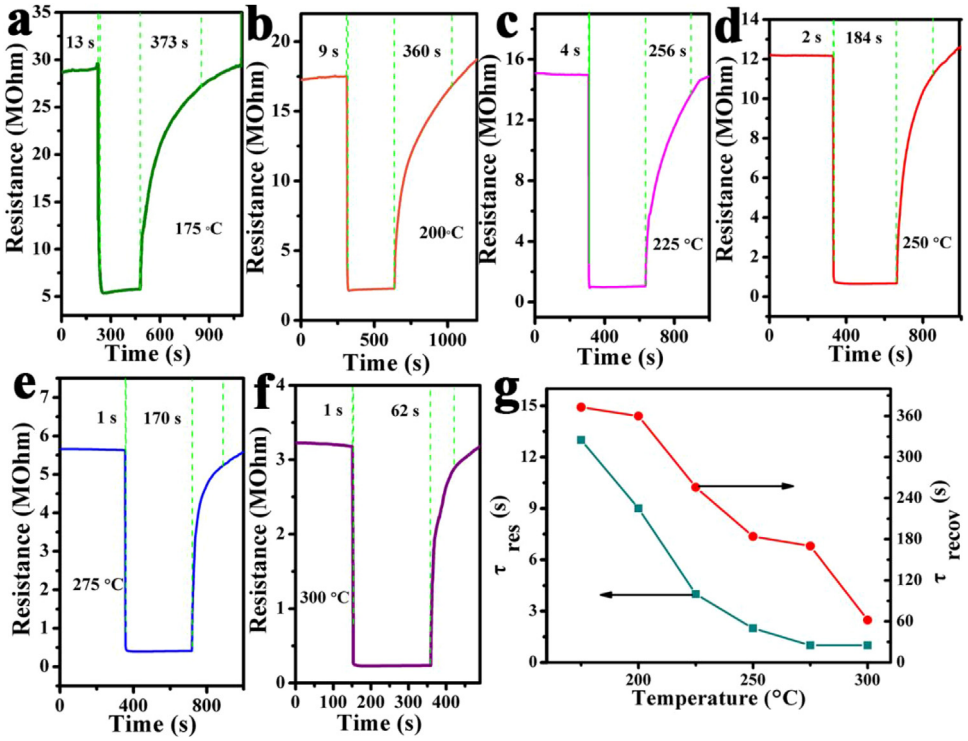

Fig. 8. (a–f) Response transients of the porous SnO_2/Zn_2SnO_4 composites to 20 ppm TEA at different operating temperature. (g) Response and recovery times of the sensor based on SnO_2/Zn_2SnO_4 composites at different operating temperature.

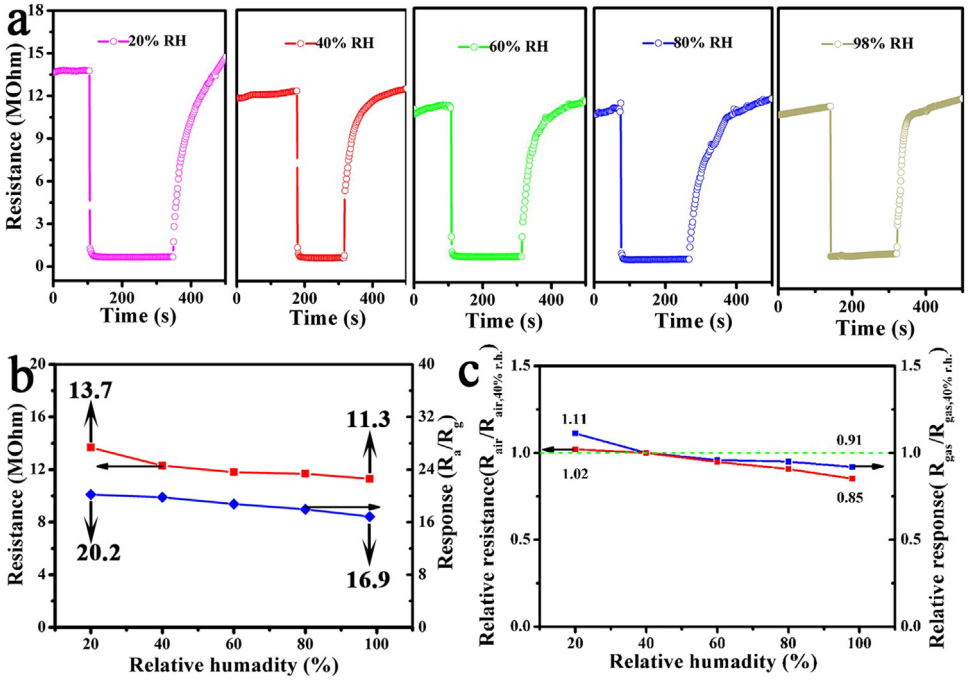

Fig. 9. (a) Dynamic response curves of SnO_2/Zn_2SnO_4 sensor to 20 ppm TEA under various humidity (20%–98% RH) at 250 °C, (b-c) Corresponding resistance and response changes with increasing humidity.

and leads to a reduction in the depletion layer, and consequently, to a decrease in the sensor resistance [40–42]. Moreover, under high RH, the TEA molecules compete with water vapor for adsorbed oxygen ions on the surface of sensing material, which contribute to a lower response to TEA under wet conditions [43].

Fig. 10a is the continuous response of the SnO_2/Zn_2SnO_4 sensor to 20 ppm TEA at 250 °C. The ten reversible cycles of the response curves at 250 °C showed almost unchanged response, indicating an excellent repeatability of the sensor. In order to further evaluate the long-term stability of the sensor, the response of the sensor to 20 ppm TEA at 250 °C was measured during 30 days, as shown in Fig. 10b and c. Although, the resistance and response of the sensor changed every day, there was no obvious fluctuation in the resistance and response values during the test days, which indicated that the sensor based on the porous SnO_2/Zn_2SnO_4 spheres had a good stability.

3.3. Gas sensing mechanism

Zn_2SnO_4 and SnO_2 are well-known *n*-type semiconductor metal oxides. A popular and widely accepted sensing mechanism for *n*-type semiconductor oxides is based on the space-charge layer mode [44,45], which is based on the change in resistance of the sensor exposed to different gas atmospheres. When the sensor is exposed to ambient air, oxygen molecules adsorb on the surface of SnO_2/Zn_2SnO_4 composite and trap free electrons from the conduction band of the sensing materials to form surface adsorbed oxygen species, including O_2^-(ads), O^-(ads), O^{2-}(ads) [46]. As a result, electron depletion layers are formed on the surface of the SnO_2/Zn_2SnO_4 composite, resulting in a reduction of the carrier concentration. When the sensor is exposed to reductive gas, for instance, TEA, at a moderate temperature, the gas will react with adsorbed oxygen species on the surface of SnO_2/Zn_2SnO to form CO_2, H_2O and N_2 [46–48]. During this process, the captured electrons will be released back into the conduction band. This process narrows the width of the depletion layer, resulting in increased electrical conductance and decreased resistance of SnO_2/Zn_2SnO_4 sensor.

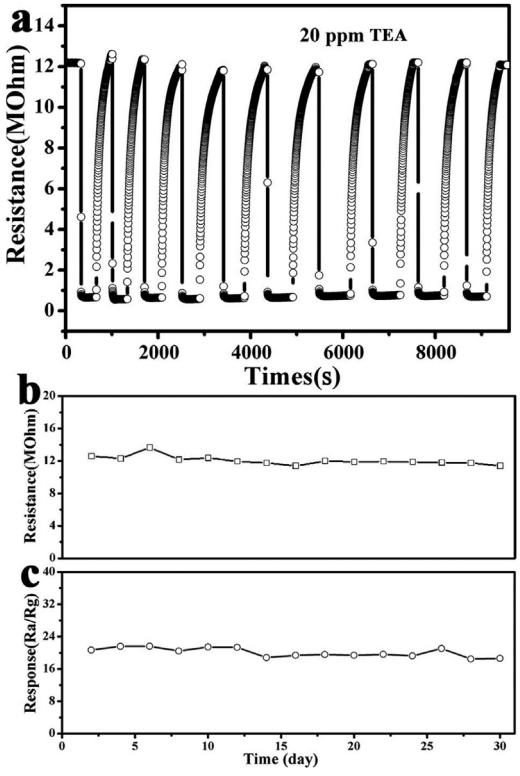

Fig. 10. (a) Ten cycles of dynamic response curves of SnO_2/Zn_2SnO_4 sensor to 20 ppm TEA at 250 °C, (b) Resistances in air and (c) Responses to 20 ppm TEA of the SnO_2/Zn_2SnO_4 sensor as a function of the test days at 250 °C.

The excellent gas sensing performances of the sensor based on the porous SnO_2/Zn_2SnO_4 spheres are mainly attributed to

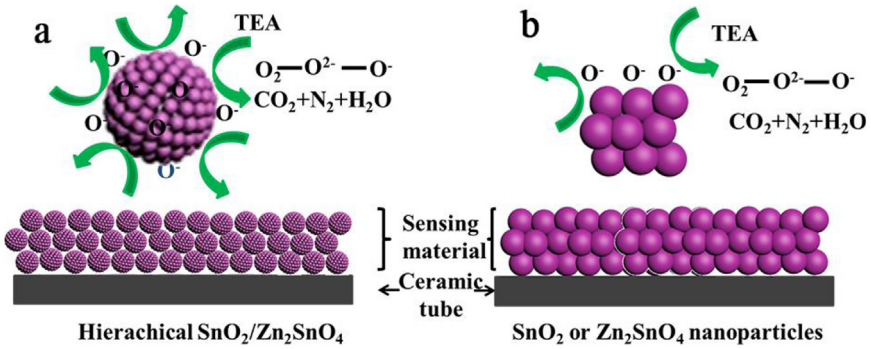

Fig. 11. Schematic diagram of the TEA sensing mechanism of (a) SnO_2/Zn_2SnO_4 porous sphere and (b) SnO_2 or Zn_2SnO_4 nanoparticles.

the porous architecture and the formation of the heterojunctions between SnO_2 and Zn_2SnO_4. Firstly, the porous SnO_2/Zn_2SnO_4 composite are composed of numerous SnO_2 and Zn_2SnO_4 nanoparticles. As illustrated in Fig. 11a and b, the hierarchical structure and porous surface can provide a higher accessible surface area and facilitate the diffusion of oxygen and tested gases (Fig. S2 and Table S1). Therefore, more surface active sites are available for sensing reactions between the adsorbed negatively charged oxygen ions species and tested gas molecules. Then the utilization rate of the sensing body is increased thus the gas sensing performance is improved. While for the pure SnO_2 and Zn_2SnO_4 nanoparticles, the nanoparticles are packed tightly, and the oxygen and tested gas could only adsorb on the surface of the sensing body resulting in a low utilization of the sensing body, and a relatively lower sensing response.

Another reason is the existence of SnO_2/Zn_2SnO_4 heterojunctions which will make a significant contribution to the enhancement of the gas sensing performance [49,50]. When Zn_2SnO_4 is doped with SnO_2, the electrons can be transferred between these two semiconductors because of their different band gap energy and work function. Therefore, SnO_2/Zn_2SnO_4 heterojunctions are created between SnO_2 and Zn_2SnO_4. Due to the conduction band edge of Zn_2SnO_4 locates at higher potential than that of SnO_2, and the electrons in the conduction band of Zn_2SnO_4 will migrate to the conduction band of SnO_2 [51] until their Femi level become equal. And an additional electron depletion layer will generated in the interface of SnO_2/Zn_2SnO_4 composites, which will play an important role in the sensing reactions, and resulting in an enhanced sensing performance.

4. Conclusions

In summary, a facile one-step hydrothermal method combined with subsequent calcination process was developed for the synthesis of porous SnO_2/Zn_2SnO_4 spheres. The as-prepared product was utilized as sensing material for the fabrication of gas sensor, and the sensing properties were systematically investigated. The results indicated that compared with pure SnO_2 and Zn_2SnO_4 solid particles, the sensor based on porous SnO_2/Zn_2SnO_4 spheres showed rapid response, good repeatability and high selectivity toward TEA. And the detection limit was 500 ppb with a response value of 1.4. The good sensing property of SnO_2/Zn_2SnO_4 samples is attributed to the porous architecture as well as the existence of SnO_2/Zn_2SnO_4 heterojunctions. The SnO_2/Zn_2SnO_4 spheres show a good potential for the applications of TEA gas sensor.

Acknowledgements

This work is supported by the National Key Research and Development Program of China (No. 2016YFC0207300). National Nature Science Foundation of China (Nos. 61722305, 61503148, 61520106003, 61327804). Science and Technology Development Program of Jilin Province (No. 20170520162JH). China Postdoctoral Science Foundation funded project Nos. 2017T100208 and 2015M580247.

Appendix A. Supplementary data

Supplementary data associated with this article can be found, in the online version, at https://doi.org/10.1016/j.snb.2018.03.044.

References

[1] D. Ju, H. Xu, Q. Xu, H. Gong, Z. Qiu, J. Guo, J. Zhang, B. Cao, High triethylamine-sensing properties of NiO/SnO2 hollow sphere P-N heterojunction sensors, Sens. Actuators B: Chem. 215 (2015) 39–44.
[2] B. Liu, L. Zhang, H. Zhao, Y. Chen, H. Yang, Synthesis and sensing properties of spherical flowerlike architectures assembled with SnO2 submicron rods, Sens. Actuators B: Chem. 173 (2012) 643–651.
[3] L. Xu, H. Song, J. Hu, Y. Lv, K. Xu, A cataluminescence gas sensor for triethylamine based on nanosized LaF3-CeO2, Sens. Actuators B: Chem. 169 (2012) 261–266.
[4] B. Akesson, S. Skerfving, L. Mattiasson, Experimental study on the metabolism of triethylamine in man, Br. J. Ind. Med. 45 (1988) 262–268.
[5] E. Filippo, D. Manno, A. Buccolieri, A. Serra, Green synthesis of sucralose-capped silver nanoparticles for fast colorimetric triethylamine detection, Sens. Actuators B: Chem. 178 (2013) 1–9.
[6] W.M. Moore, R.J. Edwards, L.T. Bavda, An improved capillary gas chromatography method for triethylamine. Application to sarafloxacin hydrochloride and GnRH residual solvents testing, Anal. Lett. 32 (1999) 2603–2612.
[7] J.F. Haskin, G.W. Warren, L.J. Priestley, V.A. Yarborough, Gas chromatography. determination of constituents in study of azeotropes, Anal. Chem. 30 (1958) 217–219.
[8] N. Yamazoe, Toward innovations of gas sensor technology, Sens. Actuators B: Chem. 108 (2005) 2–14.
[9] P. Sun, Y. Cao, J. Liu, Y. Sun, J. Ma, G. Lu, Dispersive SnO2 nanosheets: hydrothermal synthesis and gas-sensing properties, Sens. Actuators B: Chem. 156 (2011) 779–783.
[10] S.-J. Kim, I.-S. Hwang, J.-K. Choi, Y.C. Kang, J.-H. Lee, Enhanced C2H5OH sensing characteristics of nano-porous In2O3 hollow spheres prepared by sucrose-mediated hydrothermal reaction, Sens. Actuators B: Chem. 155 (2011) 512–518.
[11] S. Xu, Z.L. Wang, One-dimensional ZnO nanostructures: solution growth and functional properties, Nano Res. 4 (2011) 1013–1098.
[12] D.R. Miller, S.A. Akbar, P.A. Morris, Nanoscale metal oxide-based heterojunctions for gas sensing: a review, Sens. Actuators B: Chem. 204 (2014) 250–272.
[13] J.-H. Lee, Gas sensors using hierarchical and hollow oxide nanostructures: overview, Sens. Actuators B: Chem. 140 (2009) 319–336.
[14] X. Hu, G. Li, J.C. Yu, Design, Fabrication, and modification of nanostructured semiconductor materials for environmental and energy applications, Langmuir 26 (2010) 3031–3039.
[15] X. Liu, T. Ma, N. Pinna, J. Zhang, Two-dimensional nanostructured materials for gas sensing, Adv. Funct. Mater. 27 (2017).
[16] B. Tan, E. Toman, Y. Li, Y. Wu, Zinc stannate (Zn2SnO4) dye-sensitized solar cells, J. Am. Chem. Soc. 129 (2007) 4162–4163.
[17] A. Bera, A.D. Sheikh, M.A. Haque, R. Bose, E. Alarousu, O.F. Mohammed, T. Wu, Fast crystallization and improved stability of perovskite solar cells with Zn2SnO4 electron transporting layer: interface matters, ACS Appl. Mater. Interfaces 7 (2015) 28404–28411.

[18] W.-Q. Wu, D. Chen, R.A. Caruso, Y.-B. Cheng, Recent progress in hybrid perovskite solar cells based on n-type materials, J. Mater. Chem. A 5 (2017) 10092–10109.
[19] E.L. Foletto, J.M. Simoes, M.A. Mazutti, S.L. Jahn, E.I. Muller, L.S. Fagundes Pereira, E.M. de Moraes Flores, Application of Zn2SnO4 photocatalyst prepared by microwave-assisted hydrothermal route in the degradation of organic pollutant under sunlight, Ceram. Int. 39 (2013) 4569–4574.
[20] M. Ben Ali, F. Barka-Bouaifel, H. Elhouichet, B. Sieber, A. Addad, L. Boussekey, M. Ferid, R. Boukherroub, Hydrothermal synthesis phase structure, optical and photocatalytic properties of Zn2SnO4 nanoparticles, J. Colloid Interface Sci. 457 (2015) 360–369.
[21] P.P. Das, A. Roy, M. Tathavadekar, P.S. Devi, Photovoltaic and photocatalytic performance of electrospun Zn2SnO4 hollow fibers, Appl. Catal. B 203 (2017) 692–703.
[22] K. Wang, Y. Huang, H. Huang, Y. Zhao, X. Qin, X. Sun, Y. Wang, Hydrothermal synthesis of flower-like Zn2SnO4 composites and their performance as anode materials for lithium-ion batteries, Ceram. Int. 40 (2014) 8021–8025.
[23] C.T. Cherian, M. Zheng, M.V. Reddy, B.V.R. Chowdari, C.H. Sow, Zn2SnO4 nanowires versus nanoplates: electrochemical performance and morphological evolution during Li-Cycling, ACS Appl. Mater. Interfaces 5 (2013) 6054–6060.
[24] L. Qin, S. Liang, X. Tan, A. Pan, Zn2SnO4/graphene composites as anode materials for high performance lithium-ion batteries, J. Alloys Compd. 692 (2017) 124–130.
[25] X.-G. Han, X.-W. Cao, L. Li, C. Wang, Fabrication and characterization of polliwog-like Sn/Zn2SnO4 heterostructure nanocrystal and their gas sensing properties, Sens. Actuators B: Chem. 185 (2013) 383–388.
[26] Y.-Q. Jiang, C.-X. He, R. Sun, Z.-X. Xie, L.-S. Zheng, Synthesis of Zn2SnO4 nanoplate-built hierarchical cube-like structures with enhanced gas-sensing property, Mater. Chem. Phys. 136 (2012) 698–704.
[27] S. Sun, S. Liang, Morphological zinc stannate: synthesis, fundamental properties and applications, J. Mater. Chem. A 5 (2017) 20534–20560.
[28] X. Chu, R. Hu, J. Wang, Y. Dong, W. Zhang, L. Bai, W. Sun, Preparation and gas sensing properties of graphene-Zn2SnO4 composite materials, Sens. Actuators B: Chem. 251 (2017) 120–126.
[29] X. Wang, R. Cao, S. Zhang, P. Hou, R. Han, M. Shao, X. Xu, Hierarchical flowerlike metal/metal oxide nanostructures derived from layered double hydroxides for catalysis and gas sensing, J. Mater. Chem. A 5 (2017) 23999–24010.
[30] X. Wang, S. Zhang, M. Shao, J. Huang, X. Deng, P. Hou, X. Xu, Fabrication of ZnO/ZnFe2O4 hollow nanocages through metal organic frameworks route with enhanced gas sensing properties, Sens. Actuators B: Chem. 251 (2017) 27–33.
[31] L. Wang, T. Zhou, R. Zhang, Z. Lou, J. Deng, T. Zhang, Comparison of toluene sensing performances of zinc stannate with different morphology-based gas sensors, Sens. Actuators B: Chem. 227 (2016) 448–455.
[32] H.M. Yang, S.Y. Ma, H.Y. Jiao, Q. Chen, Y. Lu, W.X. Jin, W.Q. Li, T.T. Wang, X.H. Jiang, Z. Qiang, H. Chen, Synthesis of Zn2SnO4 hollow spheres by a template route for high-performance acetone gas sensor, Sens. Actuators B: Chem. 245 (2017) 493–506.
[33] S. Shu, M. Wang, Y. Wei, S. Liu, Synthesis of surface layered hierarchical octahedral-like structured Zn2SnO4/SnO2 with excellent sensing properties toward HCHO, Sens. Actuators B: Chem. 243 (2017) 1171–1180.
[34] Q. Zhao, D. Ju, X. Song, X. Deng, M. Ding, X. Xu, H. Zeng, Polyhedral Zn2SnO4: Synthesis, enhanced gas sensing and photocatalytic performance, Sens. Actuators B: Chem. 229 (2016) 627–634.
[35] W. Li, H. Xu, T. Zhai, H. Yu, Q. Xu, X. Song, J. Wang, B. Cao, High-sensitivity high-selectivity, and fast-recovery-speed triethylamine sensor based on ZnO micropyramids prepared by molten salt growth method, J. Alloys Compd. 695 (2017) 2930–2936.
[36] M. Wu, X. Zhang, S. Gao, X. Cheng, Z. Rong, Y. Xu, H. Zhao, L. Huo, Construction of monodisperse vanadium pentoxide hollow spheres via a facile route and triethylamine sensing property, CrystEngComm 15 (2013) 10123–10131.
[37] H.-Y. Yang, X.-L. Cheng, X.-F. Zhang, Z.-K. Zheng, X.-F. Tang, Y.-M. Xu, S. Gao, H. Zhao, L.-H. Huo, Novel sensor for fast detection of triethylamine based on rutile TiO2 nanorod arrays, Sens. Actuators B: Chem. 205 (2014) 322–328.
[38] Y. Zou, S. Chen, J. Sun, J. Liu, Y. Che, X. Liu, J. Zhang, D. Yang, Highly efficient gas sensor using a hollow SnO2 microfiber for triethylamine detection, ACS Sens. 2 (2017) 897–902.
[39] T. Rakshit, S. Santra, I. Manna, S.K. Ray, Enhanced sensitivity and selectivity of brush-like SnO2 nanowire/ZnO nanorod heterostructure based sensors for volatile organic compounds, RSC Adv. 4 (2014) 36749–36756.
[40] K. Grossmann, S. Wicker, U. Weimar, N. Barsan, Impact of Pt additives on the surface reactions between SnO2 water vapour, CO and H2; an operando investigation, Phys. Chem. Chem. Phys. 15 (2013) 19151–19158.
[41] D. Koziej, N. Barsan, U. Weimar, J. Szuber, K. Shimanoe, N. Yamazoe, Water-oxygen interplay on tin dioxide surface: implication on gas sensing, Chem. Phys. Lett. 410 (2005) 321–323.
[42] C.A. Zito, T.M. Perfecto, D.P. Volanti, Impact of reduced graphene oxide on the ethanol sensing performance of hollow SnO2 nanoparticles under humid atmosphere, Sens. Actuators B: Chem. 244 (2017) 466–474.
[43] M. Huebner, C.E. Simion, A. Tomescu-Stanoiu, S. Pokhrel, N. Barsan, U. Weimar, Influence of humidity on CO sensing with p-type CuO thick film gas sensors, Sens. Actuators B: Chem. 153 (2011) 347–353.
[44] R.W.J. Scott, S.M. Yang, G. Chabanis, N. Coombs, D.E. Williams, G.A. Ozin, Tin dioxide opals and inverted opals: near-ideal microstructures for gas sensors, Adv. Mater. 13 (2001) 1468–1472.
[45] H. Ogawa, M. Nishikawa, A. Abe, Hall measurement studies and an electrical conduction model of tin oxide ultrafine particle films, J. Appl. Phys. 53 (1982) 4448–4455.
[46] H. Xu, J. Ju, W. Li, J. Zhang, J. Wang, B. Cao, Superior triethylamine-sensing properties based on TiO2/SnO2 n–n heterojunction nanosheets directly grown on ceramic tubes, Sens. Actuators B: Chem. 228 (2016) 634–642.
[47] D.-X. Ju, H.-Y. Xu, Z.-W. Qiu, Z.-C. Zhang, O. Xu, J. Zhang, J.-Q. Wang, B.-Q. Cao, Near room temperature fast-response, and highly sensitive triethylamine sensor assembled with Au-Loaded ZnO/SnO2 core shell nanorods on flat alumina substrates, ACS Appl. Mater. Interfaces 7 (2015) 19163–19171.
[48] D. Ju, H. Xu, Z. Qiu, J. Guo, J. Zhang, B. Cao, Highly sensitive and selective triethylamine-sensing properties of nanosheets directly grown on ceramic tube by forming NiO/ZnO PN heterojunction, Sens. Actuators B: Chem. 200 (2014) 288–296.
[49] M. Zhao, J. Huang, Y. Zhou, X. Pan, H. He, Z. Ye, X. Pan, Controlled synthesis of spinel ZnFe2O4 decorated ZnO heterostructures as peroxidase mimetics for enhanced colorimetric biosensing, Chem. Commun. 49 (2013) 7656–7658.
[50] S. Wang, J. Zhang, J. Yang, X. Gao, H. Zhang, Y. Wang, Z. Zhu, Spinel ZnFe2O4 nanoparticle-decorated rod-like ZnO nanoheterostructures for enhanced gas sensing performances, RSC Adv. 5 (2015) 10048–10057.
[51] J. Yang, S. Wang, L. Zhang, R. Dong, Z. Zhu, X. Gao, Zn2SnO4-doped SnO2 hollow spheres for phenylamine gas sensor application, Sens. Actuators B: Chem. 239 (2017) 857–864.

Biographies

Xueli Yang received her B. Eng. degree in 2013 and M.S. degree in 2016 from College of Science, Northeast Forestry University in China. Currently she is studying for her Ph.D. degree in College of Electronic Science and Engineering, Jilin University, China. Her research interests focus on the synthesis and characterization of semiconductor oxide functional materials and gas sensors.

Qi Yu received the BS degree in Department of Electronic Science and Engineering in 2017. Now she is currently studying for her MS degree in College of Electronic Science and Engineering, Jilin University, China. Her research interests include the synthesis of functional materials and their applications in gas sensors.

Sufang Zhang received the BS degree in Department of Electronic Science and Engineering in 2017. She is currently studying for her MS degree in College of Electronic Science and Engineering, Jilin University, China. Now, her research interests include the synthesis of functional materials and their applications in gas sensors.

Peng Sun received his PhD degree from College of Electronic Science and Engineering, Jilin University, China in 2014. He was appointed the lecturer in Jilin University in the same year. Now, he is engaged in the synthesis and characterization of the semiconducting functional materials and gas sensors.

Huiying Lu received his MS degree from College of Chemistry, Jilin University, China in 2012 and received his PhD degree from College of Chemistry, Jilin University, China in 2015. He is currently studying for his post-doctoral degree in College of Electronic Science and Engineering, Jilin University, China.

Xu Yan received his M.S. degree in 2013 from Nanjing Agricultural University. He joined the group of Prof. Xingguang Su at Jilin University and received his Ph.D. degree in June 2017. Since then, he did postdoctoral work with Prof. Geyu Lu. Currently, his research interests mainly focus on the development of the functional nanomaterials for chem/bio sensors.

Fangmeng Liu received his PhD degree in 2017 from College of Electronic Science and Engineering, Jilin University, China. Now he is a lecturer of Jilin University, China. His current research interests include the application of functional materials and development of solid state electrolyte gas sensor and flexible device.

Xin zhou received his BS and MS degrees from College of Electronic Science and Engineering, Jilin University, China in 2013 and 2016, respectively. He is currently pursuing a PhD at the University of Tsukuba. His research interests focus on studying the properties of inorganic nanomaterials via *in situ* transmission electron microscope.

Xishuang Liang received the B. Eng. degree in Department of Electronic Science and Technology in 2004. He received his Doctor's degree in College of Electronic Science and Engineering at Jilin University in 2009. Now he is an associate professor of Jilin University, China. His current research is solid electrolyte gas sensor.

Yuan Gao received her PhD degree from Department of Analytical Chemistry at Jilin University in 2012. Now she is an associate professor in Jilin University, China. Her current research is focus on the preparation and application of graphene and semiconductor oxide, especial in gas sensor and biosensor.

Geyu Lu received the BS degree in electronic sciences in 1985 and the MS degree in 1988 from Jilin University in China and the Dr. Eng. degree in 1998 from Kyushu University in Japan. Now he is a professor of Jilin University, China. His current research interests include the development of chemical sensors and the application of the function materials.